



# Characteristics of earthquake source and ground motions in Northern Vietnam investigated through the 2020 Moc Chau M5.0 earthquake sequence

Cong Nghia Nguyen<sup>a,b,c</sup>, Van Duong Nguyen<sup>d,f</sup>, Le Minh Nguyen<sup>d,e</sup>, Van Bang Phung<sup>b</sup>, Bor-Shouh Huang<sup>b,\*</sup>, Nguyen Anh Duong<sup>d</sup>, Quang Khoi Le<sup>d</sup>, Thi Giang Ha<sup>d</sup>, Dinh Quoc Van<sup>d</sup>, Ha Vinh Long<sup>a,b,c,d</sup>, Po-Fei Chen<sup>c</sup>

<sup>a</sup> Taiwan International Graduate Program Earth Sciences System (TIGP-ESS), Academia Sinica and National Central University, Taiwan

<sup>b</sup> Institute of Earth Sciences, Academia Sinica, Taipei, Taiwan

<sup>c</sup> Department of Earth Sciences, National Central University, Taoyuan City, Taiwan

<sup>d</sup> Institute of Geophysics, Vietnam Academy of Science and Technology, Ha Noi, Viet Nam

<sup>e</sup> Department of International Cooperation, Vietnam Academy of Science and Technology (VAST), Viet Nam

<sup>f</sup> Graduate University of Science and Technology (GUST), Vietnam Academy of Science and Technology, Viet Nam

## ARTICLE INFO

### Keywords:

Moc Chau earthquake  
Focal mechanisms  
Strike-slip fault  
Ground motion

## ABSTRACT

On July 27, 2020, a shallow earthquake with a moment magnitude ( $M_w$ ) of 5.0 occurred near Moc Chau in Northwestern Vietnam. Several shallow aftershocks, clustered in a small area, followed the mainshock. The mainshock caused damage to infrastructure in the source area, and considerable shaking was felt in many high buildings in surrounding cities. This event was the first recorded significant earthquake by a newly operational Vietnam broadband seismic network. The ground motions of this earthquake sequence were adequately recorded by this network. The strike-slip rupture mechanisms of the events were evaluated through moment tensor inversion analysis. After this earthquake, a field survey was conducted. A combined analysis of damage patterns and source mechanisms revealed that this earthquake sequence might be associated with the active right-lateral Da River fault. The site classification of each station that recorded data on the Moc Chau series was evaluated by computing the horizontal-to-vertical spectral ratio. This earthquake sequence was analyzed to evaluate the characteristics of the earthquake source and the seismic wave propagation in Northwestern Vietnam and to address the potential earthquake engineering applications of this information.

## 1. Introduction

At 05:15 (UTC) on July 27, 2020 (local time 12:15 on July 27), an earthquake with a moment magnitude ( $M_w$ ) of 5.0 occurred near Moc Chau District, Son La Province, in the northwest region of Vietnam. The hypocenter of the mainshock was located at 20.929° N, 104.708° E (approximately 12 km from the town of Moc Chau), and had a depth of 7 km. The mainshock was followed by several aftershocks, which included two large events of  $M_w$  4.1 on July 28 and  $M_w$  4.4 on August 17. The mainshock caused moderate damage to the buildings in the nearby area; however, no loss of life was reported. The ground motions were recorded by 15 three-component stations in Northern Vietnam (Fig. 1). Most of the stations are equipped with both an accelerometer and a broadband

velocity seismometer (Lu et al., 2018; Nguyen et al., 2012). The nearest seismic station in the town of Moc Chau was less than 10 km from the epicenter of the mainshock. In this study, new archived seismic observations from the Moc Chau earthquake sequence were analyzed to identify the characteristics of the earthquake source, seismic wave propagation, and seismic hazards of the Northern Vietnam region; the potential applications of the study findings in earthquake engineering are discussed herein.

## 2. Regional tectonic setting

The tectonics of the Northern Vietnam region has been governed by the major tectonic events of the surrounding area since the Tertiary

\* Corresponding author at: Inst. Earth Sciences, Academia Sinica, P.O. BOX, 1-55, Nankang, Taipei 115, Taiwan.

E-mail address: [hwbs@earth.sinica.edu.tw](mailto:hwbs@earth.sinica.edu.tw) (B.-S. Huang).

<https://doi.org/10.1016/j.jseaes.2022.105144>

Received 9 February 2021; Received in revised form 30 January 2022; Accepted 8 February 2022

Available online 11 February 2022

1367-9120/© 2022 Elsevier Ltd. All rights reserved.

Period. The collision of India and Eurasia since 35 Ma (Tapponnier et al., 1982) has continually pushed the entire Indochina block southeastward (Huchon et al., 1994). According to GPS data, the block exhibits a crustal movement of approximately  $34.5 \pm 1$  mm/year southeastward, which is similar to the movement of the South China Block (Duong et al., 2013; Huy Minh et al., 2020; Trần et al., 2013). This has consequently led to the full development of a series of strike-slip faults in the area (Nguyen-Van et al., 2020). Geological and geophysical studies in Northern Vietnam have reported a complex regional crustal structure and several major strike-slip faults cutting the entire crust (Dinh et al., 2021; Nguyen et al., 2020; Nguyen et al., 2013). Therefore, several studies of the seismotectonics of Northern Vietnam have recommended the assessment of the seismic risk of the area (Lap, 1991; Nguyen et al., 2019; Pailoplee and Choowong, 2014; Phuong, 1991). Accordingly, researchers have comprehensively studied the most notable faults of the region (rank I; represented in Fig. 1 as thick red lines). Several minor faults (rank II) linked to rank I faults have also been identified; the notable rank II faults with potential seismic risk near the epicenter of the Moc Chau earthquake were determined to be the Da River fault and the Muong La-Bac Yen fault (Nguyen et al., 2019). On the base of analyzed reports (Nguyen and Le, 2005; Huang et al., 2009; Nguyen et al., 2019), earthquakes in the Northern Vietnam region can be characterized as shallow. Seismic events with magnitudes  $>5.0$  are related to major faults (rank I), and events with magnitudes  $<5.0$  are related to minor faults (rank II) (Nguyen et al., 2019). Previous studies have indicated the

possibility for destructive earthquakes with maximum magnitudes higher than 6 in the Northern Vietnam region (Das, 2015; Duan et al., 2013; Lu et al., 2016; Robinson et al., 2010). Two strong earthquakes have already occurred in Northwestern Vietnam in the last century (Fig. 1). The 1935 Dien Bien earthquake with a surface-wave magnitude ( $M_s$ ) of 6.8 and the 1983 Tuan Giao earthquake with a  $M_s$  of 6.7 both caused considerable infrastructural damage and loss of human life (Duong et al., 2013; Tuyen and Lu, 2012). In recent years, proposals have been presented to develop strategies for the reduction of seismic hazards (Tran and Kiyomiya, 2012, 2013; Nguyen et al., 2012). However, only limited local data are available for the assessment of ground motion behavior. In this study, data from the Moc Chau earthquake sequence allowed for the evaluation of ground motion behavior and proposal of seismic hazard reduction measures.

### 3. Identification of damage and intensity

The Moc Chau earthquake sequence caused considerable damage to the infrastructure in the surrounding area (Fig. 2), including falling bricks, cracks in walls and floors, and collapse of roofs. Minor injuries were reported; however, no loss of human life was reported. Because the earthquake's magnitude was only classified as medium, the amount of infrastructural damage suggests that buildings in Vietnam are generally prone to earthquake damage. During the Moc Chau earthquake, people in near-source regions and several sites of tall buildings in the nearby

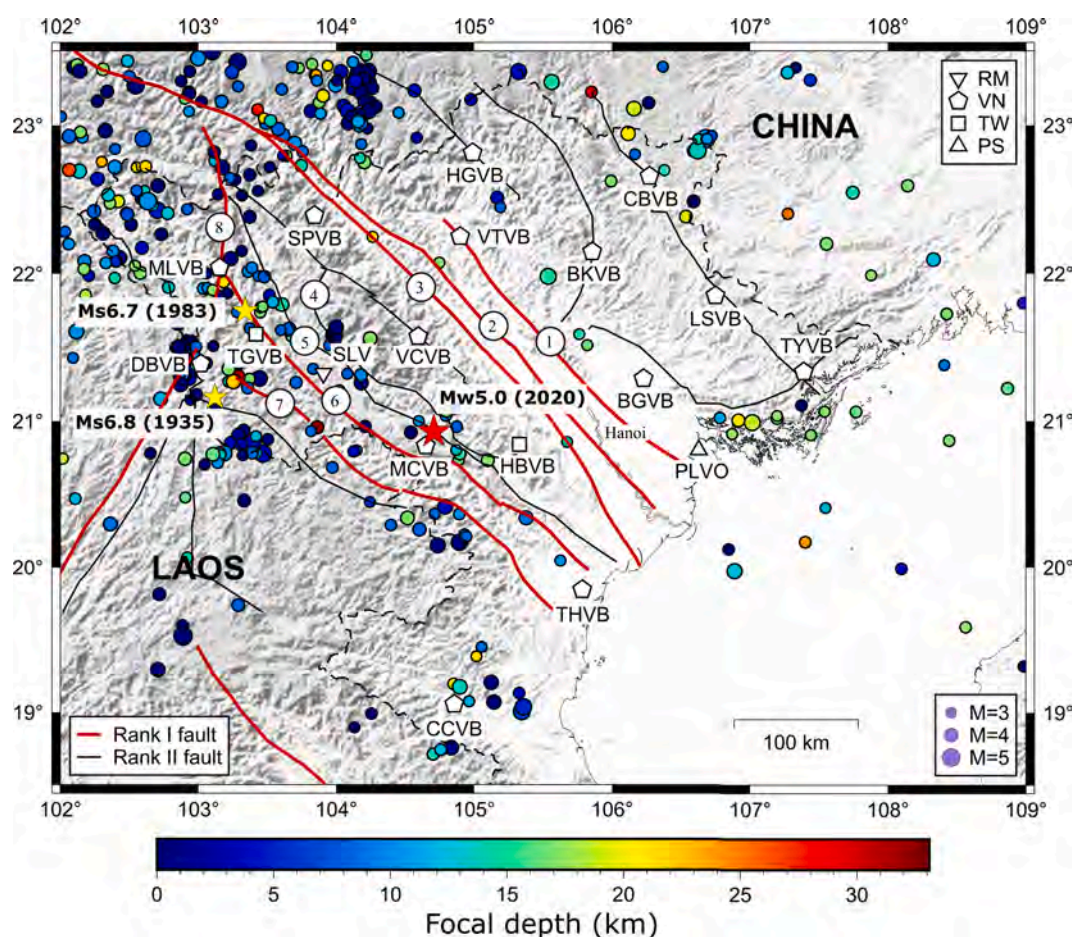


**Fig. 1.** Map of seismicity (source depths are defined by scale bar) in the Northern Vietnam region from 1990 to the present. White symbols denote seismic stations from four different networks (17 stations): Vietnam National network (VN), Academia Sinica-Taiwan (TW) (Huang et al., 2009), Regional Integrated Multi-Hazard Early Warning System (RM), and Pacific21 (PS). Ground motions of the earthquake sequence were recorded by 15 stations; two stations (TGVB and PLVO) were not operational during the period. Numbers indicate faults: (1) Lo River fault, (2) Chay River fault, (3) Red River fault, (4) Muong La-Bac Yen fault, (5) Da River fault, (6) Son La fault, (7) Ma River fault, and (8) Dien Bien Phu fault. Fault types of rank I and II are described in the text. (For interpretation of the references to colour in this figure legend, the reader is referred to the web version of this article.)

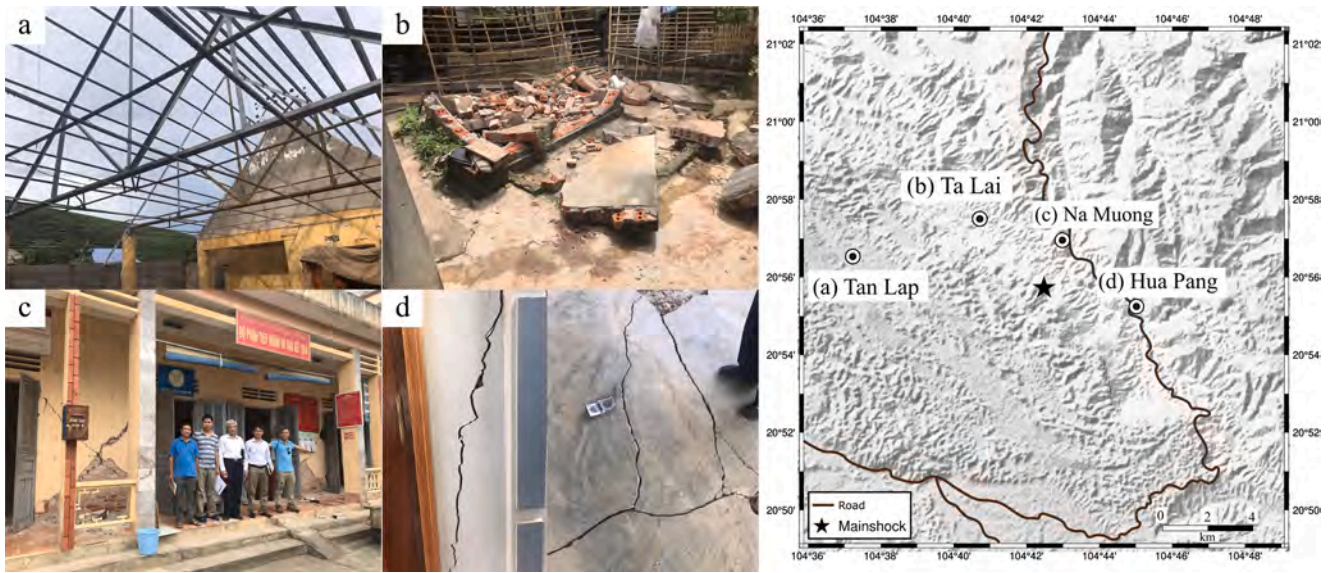


**Fig. 2.** Photos of damaged infrastructure near the mainshock within a radius of 5 km from the epicenter: a) roof collapse due to the earthquake shaking, b) falling bricks from a local building, c) damage to the wall of the administration center of Na Muong commune (approximately 2.6 km from the earthquake location), and d) cracks in walls and floors. Map of the locations where the photos were taken.

cities felt significant shaking. According to the records of the United States Geological Survey response website for earthquakes (<https://earthquake.usgs.gov/earthquakes/eventpage/us6000b4kv/dyfi/intensity>), 31 local witnesses, in response to the question “Did you feel it?”, reported having felt the Moc Chau earthquake at Modified Mercalli Intensity III. Most responses were from witnesses in the city of Hanoi, which is approximately 100 km away from the epicenter (Fig. 1). To identify the seismic intensity in the source area, the Institute of Geophysics (IGP) at the Vietnam Academy of Science and Technology conducted an interview survey in the near-source region and gathered 95 responses from people within a 60-km radius of the epicenter. The Medvedev-Sponheuer-Karnik scale (Medvedev and Sponheuer, 1969) was used to evaluate the intensities through interviewing witnesses’ reports of earthquake ground shaking (Fig. 3). These data points were contoured to create an isoseismal map, which revealed intensities

ranging from III to VII. The distribution of the estimated individual intensity points and the pattern of the isoseismal map demonstrated the orientation of the intensity to be elongated from the epicenter toward the northwest-southeast, following the strike direction of the Da River fault.

#### 4. Analysis and results

##### 4.1. Earthquake source characteristics

In this study, all recorded broadband seismic data of the Moc Chau earthquake sequence were converted into the SEISAN format (Havskov and Ottemöller, 1999) for further data processing. To analyze the earthquake sequence, all phase arrival times from the selected events were manually identified. Earthquake events were initially located

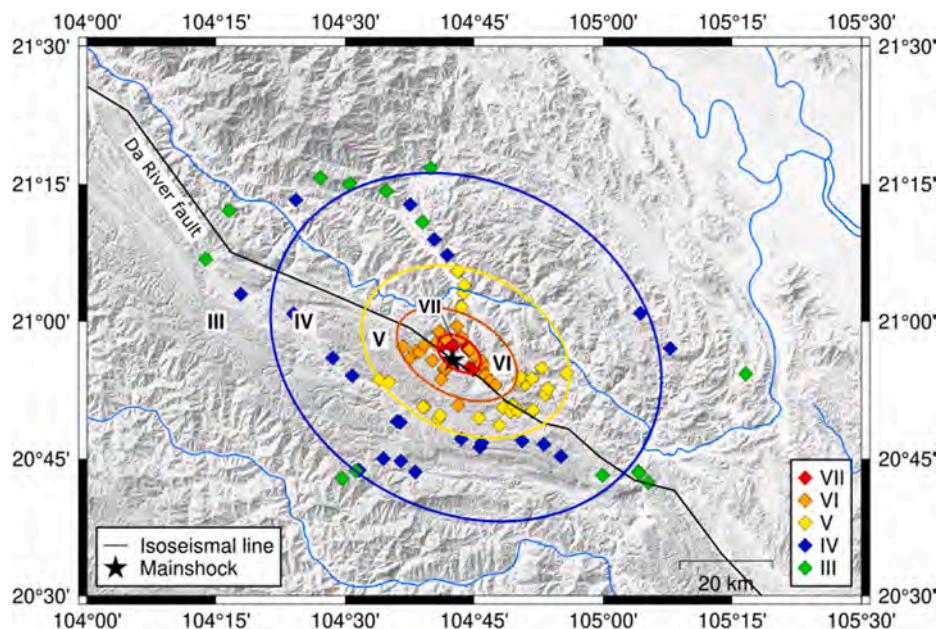


**Fig. 3.** Converted intensity from field survey after the mainshock and isoseismal line inferred from the survey points.

through the HYPOCENTER method (Lienert and Havskov, 1995) by using a one-dimensional (1D) P-wave velocity model (Table 1) and a constant  $V_p/V_s$  ratio of 1.71 based on a combination of local and regional velocity models (Huang et al., 2013; Nguyen et al., 2013; Nguyen et al., 2020). This model is currently used by IGP to locate earthquakes in Northern Vietnam. We examined the location, time residual, and location error on each event after the initial location. If the time residual or location is large, we checked the phase pick and re-picked if necessary, and located the earthquake again using the same method. Location errors for earthquakes were determined as standard errors in depth (ERZ), standard errors in epicenter (ERH), and the root mean square of travel time residuals (RMS). Table 2 lists the final location and estimation errors in the analysis of the events of the Moc Chau earthquake sequence. The errors were relatively small, with an average ERH of 3.05 km, average ERZ of 2.33 km, and average RMS of 0.33 s.

We applied the Bayesian ISOLA method (Vackár et al., 2017) to determine the focal mechanisms of the Moc Chau earthquake sequence with  $M_w$  of  $> 3$  (Table 2). In this study, moment tensors were determined using waveform fitting between broadband velocity data and synthetic seismograms through full-waveform inversion at 0.02–0.2 Hz. Fig. 4 presents the moment tensor solution of the  $M_w$  5.0 mainshock determined by fitting velocity seismograms from 12 stations. To determine the point source moment tensor solution, we inverted long-period signals of broadband waveforms by using synthetic Green's functions for compatible frequency content. Based on the results, we rejected records from a near-source station (MCVB) that were dominated by high-frequency signals as well as those from two other stations (the near-coastal station THVB and BGVB, which had thick sediment) with significant local site effects. Apart from the records obtained from the three aforementioned stations, the waveforms of the records from the other stations exhibited a reasonable fit.

The focal mechanism of the mainshock determined by our study was compared with those determined by the Thai Meteorology Department (TMD), United States Geological Survey (USGS), and Global Centroid Moment Tensor (GCMT) catalog (Table 2 and Fig. 4c). Overall, these focal mechanism solutions were consistent, presenting nearly vertical strike-slip ruptures.

Table 2 lists the moment tensor solutions determined for the 12 aftershocks ( $3.0 \leq M_w \leq 4.4$ ) of the Moc Chau earthquake. The focal mechanisms of all aftershocks were determined to be similar to those of the mainshock. Fig. 5a illustrates a plot of the distribution of these aftershocks; the focal mechanisms exhibited a possible northwest-southeast orientation along the Da River fault, which is a dextral strike-slip fault (Dinh et al., 2018). In Fig. 5b, we plotted aftershock hypocenters in a cross-section perpendicular to the Da River fault (green line in Fig. 5a). All aftershocks were shallow earthquakes with depths of  $< 10$  km and were adequately aligned in the vertical cross section. In terms of spatial distribution, these events exhibited a nearly vertical extension from the fault surface trace, indicating a nearly vertical fault plane (Fig. 5b, dashed line). The distribution of these events fits well with one of the fault planes of those focal mechanism solutions. Accordingly, we speculated that the likely rupture fault was a near-vertical dextral fault striking in the northwest-southeast direction and that the Moc Chau earthquake sequence was characterized by dextral

strike-slip events related to the activation of the Da River fault. To further investigate the mechanism of the earthquake sequence, we employed Vavryčuk, (2014) procedure to calculate the principal axes of each event. The software proposed by Vavryčuk, (2014) reads the focal mechanism of each earthquake and calculates the corresponding P-, T-, and B-axes of each event and the best-fitted  $\sigma_1$ ,  $\sigma_2$ , and  $\sigma_3$  stress directions. Fig. 5a and Fig. 6 present the P- and T-axes of the analyzed events while the principal stress directions are shown in Fig. 6.

#### 4.2. Ground motion attenuation model assessment

The Moc Chau earthquake has been the largest recorded local earthquake since the deployment of a broadband seismic network in Vietnam (Huang et al., 2009; Lu et al., 2018). Through this network, high-quality seismograms of the Moc Chau earthquake and its aftershocks could be recorded. Furthermore, the seismic stations adequately covered the locations of this sequence, thereby providing improved access to data on the ground motion properties within the station network. In this study, we collected 49 three-component seismograms of the mainshock ( $M_w = 5.0$ ) and three aftershocks ( $M_w = 3.1, 4.1, \text{ and } 4.4$ ) recorded by the 15 stations; these seismograms had a high signal-to-noise ratio and were used for further analysis.

We calculated the pseudo-spectral acceleration (PSA) of a 5% damped single-degree-of-freedom oscillator, which is a commonly used intensity measure for hazard assessment. We computed peak ground acceleration (PGA) and 5% damped PSA data in 105 oscillation periods ranging from 0.01 to 10 s for each component of a ground motion acceleration time series (one vertical and two horizontal). The geometric mean of the observed horizontal motion components was then calculated. The ratios of the horizontal to the vertical spectra were also estimated to identify the site characteristics on the basis of the dominant frequency of a given station.

The recorded PGA values were compared with those predicted using the attenuation equations proposed by Nguyen et al. (2012; hereafter N12) and Tran and Kiyomiya, (2012; hereafter TK12). The N12 and TK12 equations are both considered simplified ground motion prediction equations (GMPEs) and were developed using Vietnamese earthquake data. We calculated the epicentral distance for each record, retrieved its horizontal PGA value, and plotted attenuation curves for both GMPEs. Fig. 7 presents a comparison of the observed ground motions with the N12-predicted (solid curve) and TK12-predicted (dashed curve) ground motions caused by the mainshock (Fig. 7a) and three aftershocks (Fig. 7b) of the Moc Chau series. The observed PGA revealed a clear distance attenuation between stations. The N12-predicted ground motions generally exhibited good agreement with the observed data for all four events. Although the same events were used, the TK12-predicted ground motions were significantly greater than the N12-predicted ground motions.

#### 4.3. Seismic site condition classification

Similar to earthquake source and path effects, seismic site effects play a major role in determining the characteristics of strong ground motions (Boore, 2003; Bindi et al., 2014). The shear wave velocity in the upper 30 m ( $V_{S30}$ ) has been widely used in GMPEs and building codes as a parameter for determining site conditions. However, information on the  $V_{S30}$  of the Vietnam region is limited; therefore, most studies have used a constant  $V_{S30}$  value for GMPEs (Tran and Kiyomiya, 2012, 2013). Recently, to facilitate the employment of GMPEs, the horizontal-to-vertical spectral ratio (HVSr) has been documented for classifying sites and estimating the  $V_{S30}$  range (Di Alessandro et al., 2012; Zhao et al., 2006). In this study,  $V_{S30}$  was determined through a similar procedure. As mentioned, most of the stations record earthquakes through two types of sensors: broadband velocity seismometers record velocity seismograms, and accelerometers record acceleration seismograms. Because the broadband velocity seismometers (high-gain channels) have

**Table 1**  
Employed 1D velocity model for locating earthquakes in this study.

Layer (km)	P-wave velocity (km/s)
0–4	5.86
4–14	5.94
14–18	6.22
18–30	6.24
30–50	7.80

**Table 2**  
Source parameters of the Moc Chau earthquake sequence.

Event id	$M_L$	$M_w$	Location	Depth (km)	ERH (km)	ERZ (km)	RMS (s)	Nodal plane 1	Nodal plane 2	Moment tensor method/ Author
202,007,270,514 (Main shock)	5.0	5.0	20.929°N 104.708°E	7.1	2.4	2.1	0.5	115/84/- 173	24/83/61	(1)
		4.9	20.863°N 104.624°E	10.0				217/61/25	115/69/148	(2)
		5.0	21.11°N 104.80° E	5.0				299/51/177	32/87/39	(3)
		5.0	20.94°N 104.74° E	13.1				119/77/167	212/78/63	(4)
202,007,270,537	3.1	3.0	20.929°N 104.683°E	6.8	2.0	1.3	0.43	129/78/- 179	39/89/-12	(1)
202,007,270,850	3.4	3.4	20.930°N 104.714°E	4.1	3.9	3.9	0.16	122/80/- 179	32/89/-10	(1)
202,007,270,915	3.3	3.1	20.928°N 104.708°E	6.1	2.3	1.5	0.36	16/81/-25	111/65/- 170	(1)
202,007,272,316	3.4	3.3	20.926°N 104.725°E	1.9	6.7	4.3	0.05	305/89/173	35/83/1	(1)
202,007,280,125	4.1	4.1	20.910°N 104.716°E	5.3	3.9	3.4	0.13	26/90/-7	116/83/- 180	(1)
202,007,280,500	3.1	3.0	20.913°N 104.703°E	7.8	2.6	1.9	0.4	304/85/167	36/77/5	(1)
202,007,281,107	3.4	3.3	20.925°N 104.708°E	7.0	3.0	3.4	0.1	129/83/- 176	38/86/-7	(1)
202,007,281,326	3.5	3.3	20.925°N 104.716°E	6.1	2.3	1.5	0.49	308/90/174	38/84/0	(1)
202,008,031,015	3.4	3.4	20.911°N 104.734°E	6.6	2.5	1.3	0.45	121/75/178	212/88/15	(1)
202,008,041,525	3.4	3.0	20.928°N 104.686°E	10.1	2.7	1.4	0.39	103/74/170	196/80/17	(1)
202,008,062,328	3.0	3.3	20.933°N 104.693°E	10.0	2.5	1.8	0.34	190/89/31	100/59/179	(1)
202,008,170,113	4.4	4.4	20.907°N 104.749°E	6.9	2.9	2.5	0.55	15/73/-26	113/66/- 161	(1)

(1) Bayesian ISOLA full waveform inversion (Vackar et al., 2017)/ this study.

(2) Body-wave moment tensor/ USGS.

(3) Body-wave moment tensor, TMD.

(4) GCMT solution.

greater sensitivity than the accelerometers (low-gain channels), we used broadband velocity seismograms in place of acceleration seismograms, which have previously been commonly used by earthquake engineering as tools for estimating site conditions. Therefore, using broadband velocity seismograms, the ground motion from small events can be well recorded to analyze and to add to the databases. According to Zhao et al. (2006), the soil at a site can be classified as rock, hard soil, medium soil, or soft soil on the basis of information on the predominant period (Tg) and the peak HVSR, both of which can be determined from seismic records. Tg can be set to < 0.2 s for a rock site, to 0.2–0.4 sec for a hard-soil site, to 0.4–0.6 s for a medium-soil site, and  $\geq$  0.6 s for a soft-soil site (Zhao et al., 2006). In this study, the soil types were defined according to the specifications of Zhao et al. (2006). Fig. 8 illustrates four typical sites in Northern Vietnam classified according to Tg and the peak HVSR. It is noted that the sites under consideration of at least 3 recordings whose peak of the HVSR ratios are obvious in term of its amplitude and location. Table 3 presents a summary of the estimated site conditions for the stations according to the peak HVSR and related period Tg. These stations exhibit as a variety of site conditions, from soft soil ( $V_{S30} < 200$  m/s) to rock stiff soil ( $V_{S30} > 600$  m/s). These estimated site conditions of the seismic stations were applied to quantify several GMPEs.

## 5. Discussion

As presented in Fig. 6, all of the events had similar northwest-southeast P-axes and northeast-southwest T-axes on the horizontal plane. This stress pattern is consistent with previous reports of the Northern Vietnam tectonic stress field in which the maximum horizontal compression direction ranges from northwest-southeast to north–south and the maximum extension direction is northeast-southwest (Dinh et al., 2020; Zuchiewicz et al., 2013). This stress pattern of the Moc Chau

earthquake sequence was caused by the same regional stress field with the major regional large dextral faults, including the Red River fault (Zuchiewicz et al., 2013), Son La fault, and Ma River fault (Wu et al., 2018). Similar focal mechanisms and stress states were determined in the Son La and Ma River fault through a focal mechanism inversion of microseismic data (Wu et al., 2018). Similar to our results, previous geological and seismological studies (Dinh et al., 2020; Replumaz et al., 2001; Wan et al., 2016; Wu et al., 2018) have indicated that the Northern Vietnam region is under a stable stress regime that is capable of producing dominantly right-lateral strike-slip earthquakes along northwest-southeast faults.

Geological studies on the seismotectonics of Northern Vietnam have suggested that relatively strong earthquakes with magnitudes of > 6 may occur along the major faults of the area, including the Red River, Lo River, and Chay River fault (Allen et al., 1984; Phan et al., 2019; Trinh et al., 2012; Zuchiewicz et al., 2004). Moreover, minor faults including the Da River fault, are capable of producing earthquakes with a magnitude of > 5 (Phuong, 1991).

As displayed in Fig. 7, the N12 equation generally predicted the PGA of the Moc Chau earthquakes. However, as observable in the mainshock prediction, the N12 equation prediction is slightly over the PGA at the MCVB station, for which the epicentral distance was 9.7 km. The N12 equation does not account for information regarding site conditions or frequency-dependent variations of ground motion, which limits its applicability in seismic hazard studies and engineering applications. Both site condition and signal frequency are sensitive parameters to ground motion amplification and are necessary for modern GMPEs (Bommer et al., 2010). The TK12 equation has a similar limitation. Therefore, to more accurately assess the seismic hazards for Northern Vietnam, we evaluated the effects of site condition and frequency-dependent attenuation of ground motion by using the Moc

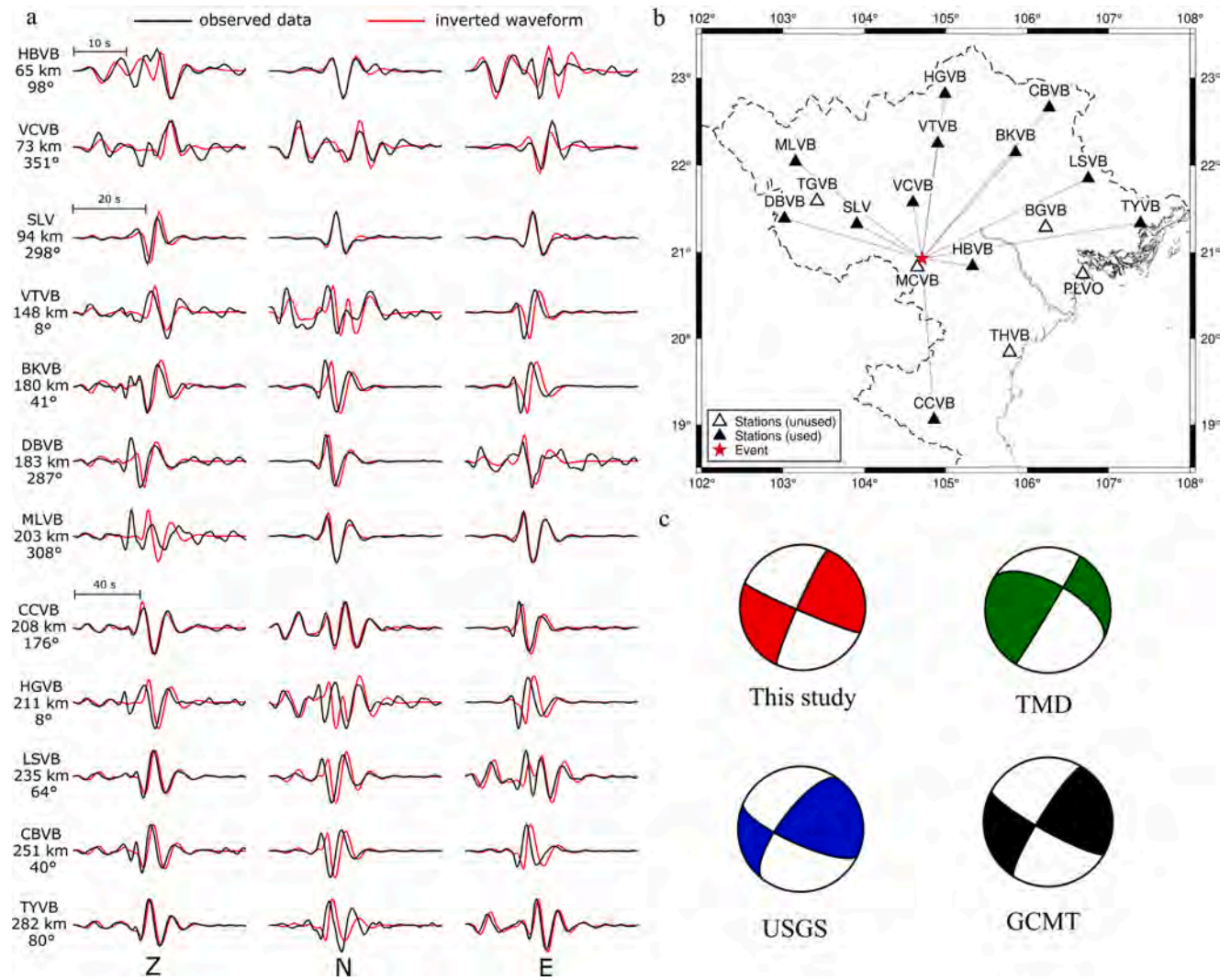


**Fig. 4.** Focal mechanism solution for the  $M_w$  5.0 Moc Chau mainshock: a) comparison between observed and synthetic waveforms for best fitting solutions; b) map of seismic stations used in moment tensor inversion; c) beachball representation of focal mechanism solutions obtained by this study, the TMD, the USGS, and the GCMT.

Chau earthquake data, and we compared our observations with those predicted using existing GMPEs.

In Vietnam, measures for the mitigation of seismic hazards in construction have recently been updated to include a seismic design code for Vietnam TCVN9386:2012 (IBST, 2012). However, to improve seismic risk preparation, a reliable GMPE is necessary. To develop such a GMPE, we compared observations obtained for the Moc Chau earthquake with site-specific predictions. The PGA and 5% damped PSA at 0.2 and 1 s were analyzed to determine the ground motions in short, middle, and long periods. We selected eight candidate GMPEs and categorized them into three groups. The first group comprised four equations, namely ASK14 (Abrahamson et al., 2014), BSSA14 (Boore et al., 2014), CB14 (Campbell and Bozorgnia, 2014), and CY14 (Chiou and Youngs, 2014), developed for global application as a part of the NGA-West2 project. The second group comprised two Taiwan-specific GMPEs, namely CH20 (Chao et al., 2020) and Ph20 (Phung et al., 2020), developed for a probabilistic seismic hazard analysis study in Taiwan (NCREE, 2015). The final group comprised two equations, namely CB08 (Campbell and Bozorgnia, 2008) and ASB14 (Akkar et al., 2014), used in a recent PSHA study in Vietnam (Truyen and Phuong, 2019).

To make predictions using the aforementioned GMPEs and compare them with the ground motion observations for the Moc Chau earthquake, source and path effects and site conditions were required as input

parameters.  $M_w$  and focal depth ( $H$ ) were adopted from moment tensor inversion. The selected GMPEs were based on two different distance metrics: the rupture distance ( $R_{rup}$ ) and Joyner-Boore distance ( $R_{jb}$ ). The ASK14, CY14, CB14, CH20, PH20, and CB08 equations were used in the  $R_{rup}$ -based models, and the BSSA14 and ASB14 equations were used in the  $R_{jb}$ -based models. Because all earthquakes considered in this study were small ( $M_w < 5$ ), we considered a point source model would be appropriate. Therefore,  $R_{rup}$  was considered to be the hypocentral distance ( $R_{hyp}$ ), and  $R_{jb}$  was considered to be the epicentral distance ( $R_{epi}$ ). In most of the GMPEs (ASK14, CY14, CB14, CH20, PH20, and CB08), the depth to the top of the rupture ( $Z_{tor}$ ) is used as an additional source parameter, and  $Z_{tor}$  can be used as the  $H$ -depth. Regarding site condition, all selected GMPEs require  $V_{S30}$  as an input; accordingly, in this study, the  $V_{S30}$  values for each site were inferred from the data presented in Table 3. The focal mechanism was set to strike-slip earthquake. All other parameters, such as the hanging-wall effect, directivity effect, and basin depth ( $Z_1$  or  $Z_{2.5}$ ), were set to their default levels (i.e., zero effect). Our analysis procedure and earthquake source parameter definitions were based on those outlined by Phung et al. (2020).

On the basis of the analysis procedure outlined by Phung et al., (2020), we visually compared the predictions obtained using the candidate GMPEs with the seismic observations for the Moc Chau earthquake sequence in terms of PGA and PSA at different oscillation

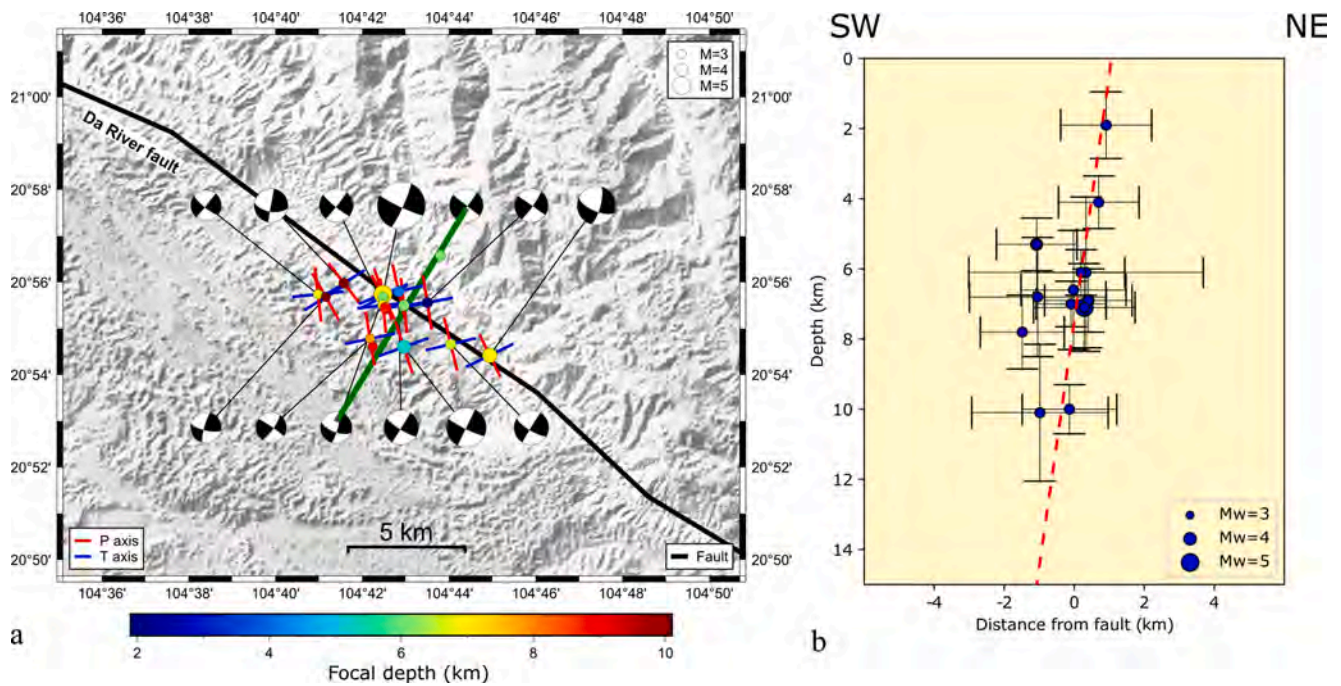


**Fig. 5.** Map of location and focal mechanism of Moc Chau earthquake sequence with magnitude of  $> 3$ : a) beachballs represent focal mechanisms of the Moc Chau earthquake sequence, with the lines indicating P- and T-axes of corresponding events; b) hypocenter locations with depth across the section (green line) of the illustration in a), with dashed line indicating possible fault plane. Error bars on each event are ERH and ERZ for horizontal and vertical axes, respectively. (For interpretation of the references to colour in this figure legend, the reader is referred to the web version of this article.)

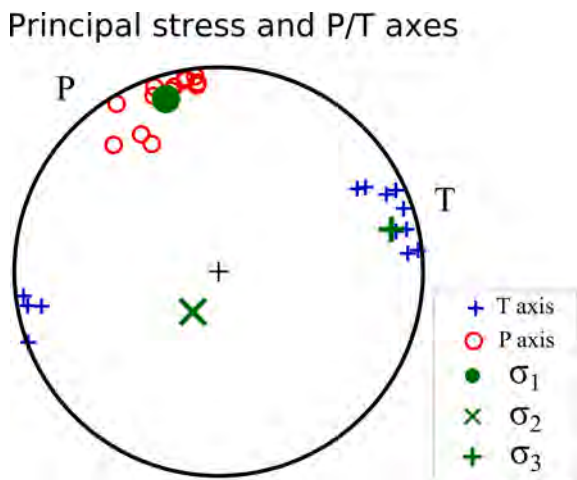


**Fig. 6.** Principal stress axes  $\sigma_1$ ,  $\sigma_2$ , and  $\sigma_3$  obtained through stress inversion using 13 focal mechanism solutions of the Moc Chau sequence. Red circles denote the P-axes for each earthquake in the sequence and blue plus symbols denote T-axes. (For interpretation of the references to colour in this figure legend, the reader is referred to the web version of this article.)

periods ( $T = 0.2$  and  $1$  s), as displayed in Fig. 9. The first panel in this figure presents the comparison results for the PGA data, and the second and third panels present the comparison results for the PSA data at oscillation periods of  $0.2$  and  $1$  s, respectively. The strong ground motions caused by the three events ( $M_w = 4.1$ ,  $M_w = 4.4$ , and the mainshock  $M_w = 5$ ) did not differ significantly at the station located at  $10$  km from the source. Notably, the candidate GMPEs were executed using the data for the  $M_w = 5$  event to compare with the main event. Overall, as presented in Fig. 9, the average PGA and PSA (at  $0.2$  s) values observed were lower than those predicted by the candidate GMPEs. However, the predictions of the candidate GMPEs exhibited a significantly poor fit with the observed data for the period  $T = 1$  s, suggesting a different rate

of distance decay in Northern Vietnam than that reported in the data of Taiwan (CH20, PH20) and California, USA (ASK14, BSSA14, CB14, and CY14). Among the candidate GMPEs, the predictions by the CH20 equation exhibited a superior fit to the data across all periods. Thus, the CH20 model was determined to be the most suitable; it had stronger attenuation and was consistent with the data.

In probabilistic seismic hazard analysis (PSHA), standard practice is to select a set of appropriate GMPEs, which describe the mean and standard deviation of ground motion in the computation procedure of PSHA. As mentioned, the CH20 model exhibited the best fit to the observations in this study. CH20 predictions with different standard deviations can be selected as input; for example, one standard deviation at  $T = 1$  s ( $\sigma = 0.75$ ) can allow for accurate estimates of ground motion levels as input for PSHA calculations. Nevertheless, for it to be applied in a PSHA study, the standard deviations of the CH20 model's predictions in different periods must be further examined. In the near future, new ground motion records in Northern Vietnam are expected to build a local GMPE; the existing model of CH20 is likely the best candidate for an initial model and is expected to predict ground motions with greater accuracy than the previous candidate GMPEs.

## 6. Conclusions

The Moc Chau earthquake sequence has provided new data for exploring the characteristics of source and ground motions in Northern Vietnam. Analyses of focal mechanisms and earthquake locations revealed the earthquake sequence to be related to the activation of the Da River fault under the stress regime of northwest-southeast to north-south maximum horizontal compression and northeast-southwest maximum extension. The results of this study also indicate that the Northern Vietnam region is under a stable stress regime that can produce dominantly right-lateral strike-slip earthquakes along the faults on northwest-southeast direction. The Moc Chau earthquake sequence serves as an example of the potential strong earthquake occurrence in Northern Vietnam.

The recorded PGA data of the 2020 Moc Chau earthquake sequence

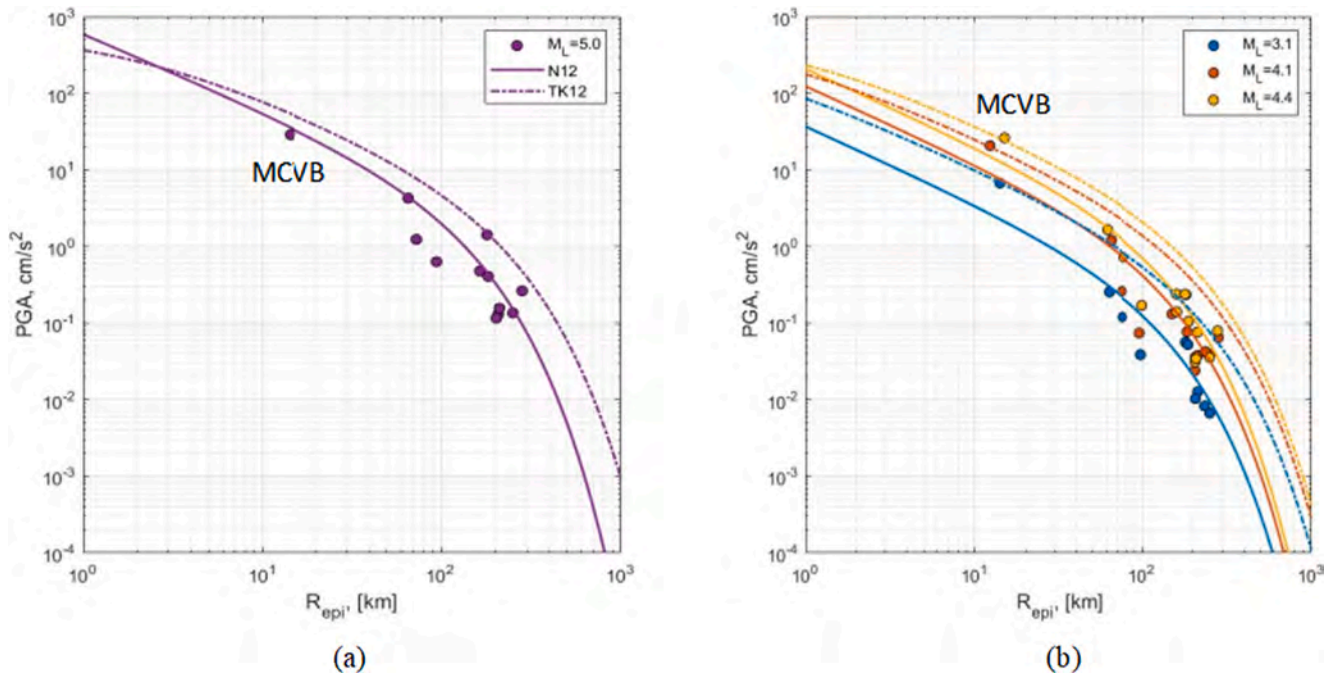


Fig. 7. Comparison of observed ground motion for PGA and those estimated through N12 and TK12 GMPEs. (a) Moc Chau mainshock ( $M_w = 5.0$ ) and (b) three aftershocks ( $M_w = 3.1, 4.1,$  and  $4.4$ ). MCVB station with epicentral distances of  $<10$  km for mainshock and its aftershocks.

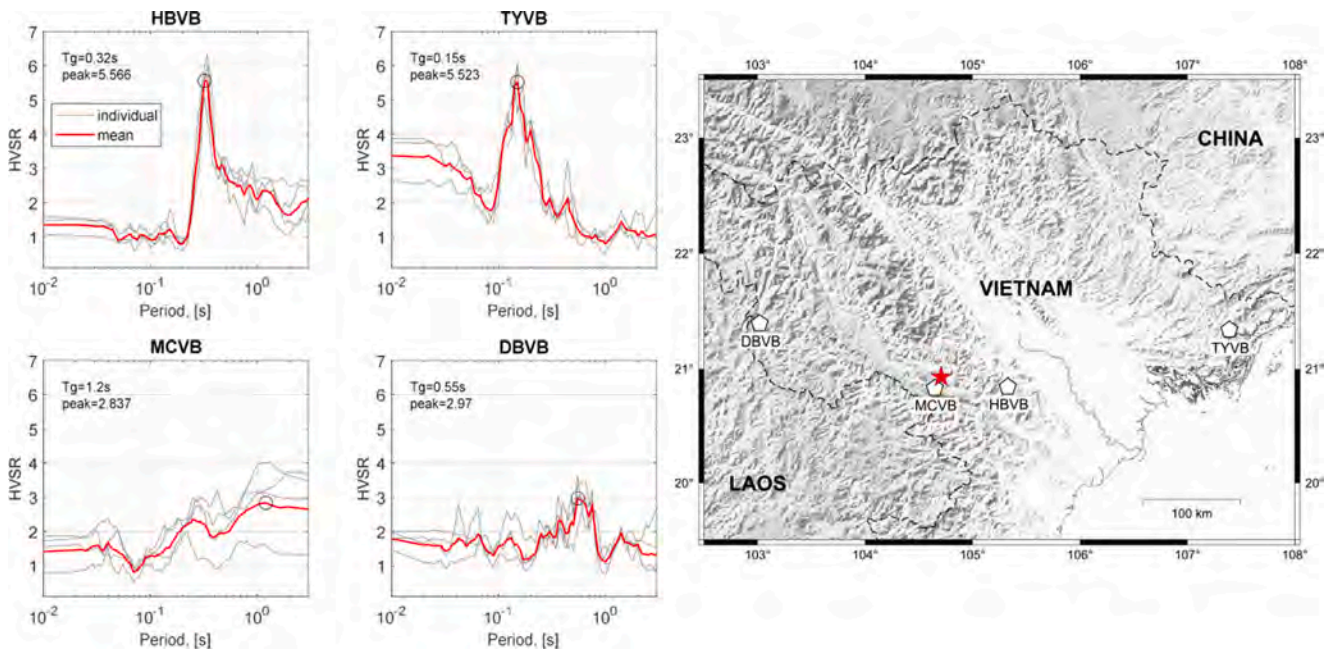


Fig. 8. HVSR values used in site classification for four typical sites in Northern Vietnam. Individual and mean HVSR values are presented in each plot. The map contains locations of seismic stations.

were compared with N12- and TK12-predicted motion. The N12-predicted ground motions generally agreed with the observed data, and the TK12-predicted motions significantly exceeded the N12-predicted motions.

We also tested eight candidate GMPEs for Northern Vietnam by using observations of the Moc Chau earthquake sequence. We performed a visual comparison of the predictions obtained by candidate GMPEs with the earthquake observations to evaluate the applicability of the GMPEs. This comparison revealed the CH20 equation to be the most suitable model among the candidates. However, an establishment of a new

GMPE for Northern Vietnam is necessary for this equation to be applicable in earthquake engineering. To achieve this, new observations and systematic analyses are required.

**CRedit authorship contribution statement**

**Cong Nghia Nguyen:** Writing – original draft, Visualization. **Van Duong Nguyen:** Conceptualization, Data curation. **Le Minh Nguyen:** Conceptualization. **Van Bang Phung:** Software. **Bor-Shouh Huang:** Writing – review & editing. **Nguyen Anh Duong:** Supervision. **Quang**

**Table 3**  
Classification of sites for each station in this study.

Station	Network	Number of Records	Peak of H/V ratio	Dominant period, Tg (s)	Zhao et al. 2006 & Alessandro et al. 2012 classification	NEHRP class	Average Vs30	Note
BGVB	VN	1	4.12	0.2	SCII:(Hard soil)	C + D	300–600 m/s	
BKVB	VN	4	3.00	0.13	SCI:(Rock Stiff soil)	A + B + C	>600 m/s	
CBVB	VN	4	2.34	0.6	SC IV: (soft soil)	D + E	<200 m/s	
CCVB	VN	4	1.28	0.1	–	–	>600	flat H/V and peak < 2
DBVB	VN	4	2.97	0.55	SC III: (Medium soil)	D	200–300 m/s	
HBVB	TW	4	5.57	0.32	SCII:(Hard soil)	C + D	300–600 m/s	
HGVB	VN	4	1.72	0.85	–	–	>600	flat H/V and peak < 2
LSVB	VN	2	2.03	0.065	SCI:(Rock Stiff soil)	A + B + C	>600 m/s	
MCVB	VN	4	2.84	1.2	–	D + E	<200	unclear peak
MLVB	VN	4	2.19	0.36	SCII:(Hard soil)	C + D	300–600 m/s	
SLV	RM	4	1.49	0.13	–	A + B + C	>600	flat H/V and peak < 2
THVB	VN	3	2.83	0.36	–	C + D	300–600 m/s	unclear peak
TYVB	VN	4	4.20	0.15	SCI:(Rock Stiff soil)	A + B + C	>600 m/s	
VCVB	VN	4	2.38	0.48	SC III: (Medium soil)	D	200–300 m/s	
VTVB	VN	1	3.17	1.1	SC IV: (soft soil)	D + E	<200 m/s	

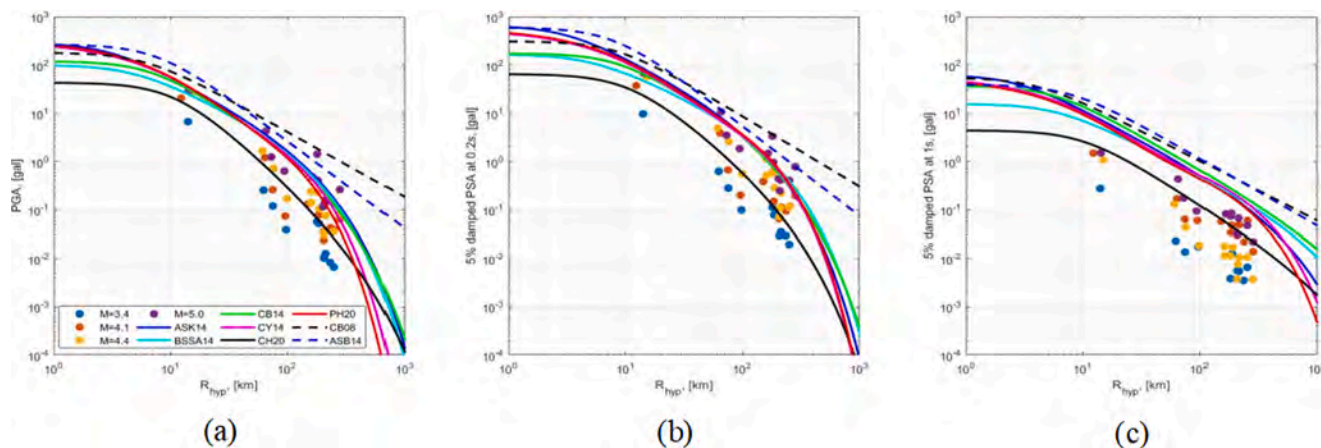


**Fig. 9.** Comparison of candidate GMPEs for PGA (a) and PSA at periods of 0.2 s (b) and 1 s (c) with observed data from the four events ( $M_w = 3.1, 4.1, 4.4, \text{ and } 5$ ). Candidate GMPEs were computed using  $M_w = 5$ .

**Khoi Le:** Data curation. **Thi Giang Ha:** Data curation. **Dinh Quoc Van:** Data curation. **Ha Vinh Long:** Data curation. **Po-Fei Chen:** Supervision.

2116-M-001-011, MOST 108-2116-M-001-010-MY3, and MOST 109-2119-M-001-011.

**Declaration of Competing Interest**

The authors declare that they have no known competing financial interests or personal relationships that could have appeared to influence the work reported in this paper.

**Acknowledgments**

We thank two anonymous reviewers for providing helpful comments on earlier drafts of the manuscript. We thank the staff of the Vietnam Academy of Science and Technology and Academia Sinica for collecting the data used in this study. We also thank Prof. T. Y. Lee for providing insightful comments and valuable feedback. This study was funded by the Vietnam National Foundation for Science and Technology Development (NAFOSTED) under grant number 01/2021/ĐX and by the Ministry of Science and Technology in Taiwan under grant MOST 108-

**References**

Abrahamson, N.A., Silva, W.J., Kamai, R., 2014. Summary of the ASK14 ground motion relation for active crustal regions. *Earthquake Spectra* 30 (3), 1025–1055.  
 Akkar, S., Sandikkaya, M.A., Bommer, J.J., 2014. Empirical ground-motion models for point-and extended-source crustal earthquake scenarios in Europe and the Middle East. *Bull. Earthq. Eng.* 12 (1), 359–387.  
 Allen, C.R., Gillespie, A.R., Yuan, HAN, Sieh, K.E., Buchun, Zhang, Chengnan, Zhu, 1984. Red River and associated faults, Yunnan Province, China: Quaternary geology, slip rates, and seismic hazard. *Geol. Soc. America Bulletin* 95 (6), 686. [https://doi.org/10.1130/0016-7606\(1984\)95<686:RRAAFY>2.0.CO;2](https://doi.org/10.1130/0016-7606(1984)95<686:RRAAFY>2.0.CO;2).  
 Bindi, D., Massa, M., Luzi, L., Ameri, G., Pacor, F., Puglia, R., Augliera, P., 2014. Pan-European ground-motion prediction equations for the average horizontal component of PGA, PGV, and 5%-damped PSA at spectral periods up to 3.0 s using the RESORCE dataset. *Bull. Earthquake Engineering* 12 (1), 391–430.  
 Bommer, J.J., Douglas, J., Scherbaum, F., Cotton, F., Bungum, H., Fäh, D., 2010. On the selection of ground-motion prediction equations for seismic hazard analysis. *Seismological Research Letters* 81(5), 783–793.  
 Boore, D.M., 2003. Simulation of ground motion using the stochastic method. *Pure Appl. Geophysics* 160 (3), 635–676.

- Boore, D.M., Stewart, J.P., Seyhan, E., Atkinson, G.M., 2014. NGA-West2 equations for predicting PGA, PGV, and 5% damped PSA for shallow crustal earthquakes. *Earthquake Spectra* 30 (3), 1057–1085.
- Campbell, K.W., Bozorgnia, Y., 2008. NGA ground motion model for the geometric mean horizontal component of PGA, PGV, PGD and 5% damped linear elastic response spectra for periods ranging from 0.01 to 10 s. *Earthquake Spectra* 24 (1), 139–171.
- Campbell, K.W., Bozorgnia, Y., 2014. NGA-West2 Ground Motion Model for the Average Horizontal Components of PGA, PGV, and 5% Damped Linear Acceleration Response Spectra. *Earthquake Spectra* 30 (3), 1087–1115.
- Chao, S.-H., Chiou, B., Hsu, C.-C., Lin, P.-S., 2020. A horizontal ground-motion model for crustal and subduction earthquakes in Taiwan. *Earthquake Spectra* 36 (2), 463–506.
- Chiou, B.-J., Youngs, R.R., 2014. Update of the Chiou and Youngs NGA model for the average horizontal component of peak ground motion and response spectra. *Earthquake Spectra* 30 (3), 1117–1153.
- Das, S., 2015. *Supershear Earthquake Ruptures-Theory, Methods, Laboratory Experiments and Fault Superhighways: An Update, Perspectives on European Earthquake Engineering and Seismology*. Springer, Cham, pp. 1–20.
- Di Alessandro, C., Bonilla, L.F., Boore, D.M., Rovelli, A., Scotti, O., 2012. Predominant-period site classification for response spectra prediction equations in Italy. *Bull. Seismological Society America* 102 (2), 680–695.
- Dinh, T.-H., Chan, Y.-C., Chang, C.-P., Chen, C.-T., Hsu, Y.-C., 2021. Deformation patterns and potential active movements of the Fansipan mountain range, northern Vietnam. *Int. J. Earth Sciences* 110 (1), 35–51.
- Dinh, V.-T., Harder, S., Huang, B.-S., Trinh, V.-B., Doan, V.-T., Lai, H.-P., Tran, A.-V., Nguyen, H.-T., Nguyen, V.-D., 2018. An overview of northern Vietnam deep crustal structures from integrated geophysical observations. *Terrestrial, Atmospheric & Oceanic Sci.* 29 (4), 371–386.
- Duan, B.V., Thang, N.C., Vuong, N.V., Nguyen, P.D., 2013. The magnitude of the largest possible earthquake in the Muong La-Bac Yen fault zone. *Vietnam J. Earth Sci.* 35, 53–59.
- Duong, N.A., Sagiya, T., Kimata, F., To, T.D., Hai, V.Q., Cong, D.C., Binh, N.X., Xuyen, N. D., 2013. Contemporary horizontal crustal movement estimation for northwestern Vietnam inferred from repeated GPS measurements. *Earth Planets Space* 65 (12), 1399–1410.
- Havskov, J., Ottemöller, L., 1999. SEISAN earthquake analysis software. *Seismol. Res. Lett.* 70 (5), 532–534.
- Huang, B.-S., Le, T.S., Liu, C.-C., Toan, D.V., Huang, W.-G., Wu, Y.-M., Chen, Y.-G., Chang, W.-Y., 2009. Portable broadband seismic network in Vietnam for investigating tectonic deformation, the Earth's interior, and early-warning systems for earthquakes and tsunamis. *J. Asian Earth Sci.* 36 (1), 110–118.
- Huang, H.-H., Xu, Z.J., Wu, Y.-M., Song, X., Huang, B.-S., Nguyen, L.M., 2013. First local seismic tomography for Red River shear zone, northern Vietnam: Stepwise inversion employing crustal P and Pn waves. *Tectonophysics* 584, 230–239.
- Huchon, P., Pichon, X.L., Rangin, C., 1994. Indochina Peninsula and the collision of India and Eurasia. *Geology* 22 (1), 27. [https://doi.org/10.1130/0091-7613\(1994\)022<0027:IPATCO>2.3.CO;2](https://doi.org/10.1130/0091-7613(1994)022<0027:IPATCO>2.3.CO;2).
- Minh, L.H., Hung, V.T., Hu, J.-C., Minh, N.L., Huang, B.-S., Chen, H.-Y., Thang, N.C., Thanh, N.H., Thanh, L.T., Mai, N.T., Hong, P.T.T., 2020. Contemporary movement of the Earth's crust in the Northwestern Vietnam by continuous GPS data. *Vietnam J. Earth Sciences* 42 (4). <https://doi.org/10.15625/0866-7187/42/4/15282>.
- IBST, 2012. TCVN9386 - Design of structures for earthquake resistances, Vietnam. Construction Publishing House: Hanoi, Vietnam, Vietnam Institute for Building Science and Technology.
- Lap, N.K., 1991. The seismotectonics of the Indochina peninsula. *J. SE Asian Earth Sci.* 6 (2), 55–61.
- Lienert, B.R., Havskov, J., 1995. A computer program for locating earthquakes both locally and globally. *Seismol. Res. Lett.* 66 (5), 26–36.
- Lu, N. T., Yu, B. V., Hang, P. T. T., Hoan, V. T., & Giang, H. T. (2018). Estimation of errors in determination of main parameters of earthquake hypocenter, recorded by the national seismic network of Vietnam. *Vietnam Journal of Earth Sciences*, 40(1), 1–16.
- Lu, N.T., Rodkin, M., Phuong, T.V., Hang, P.T.T., Quang, N., Hoan, V.T., 2016. Algorithm and program for earthquake prediction based on the geological, geophysical, geomorphological and seismic data. *Vietnam J. Earth Sciences* 38, 231–241.
- Medvedev, S., Sponheuer, W., 1969. Scale of seismic intensity. *Proc. IV World Conference of the Earthquake Engineering, Santiago, Chile, A-2*, pp. 143–153.
- National Center for Research on Earthquake Engineering (NCREE), 2015. Reevaluation of Probabilistic Seismic Hazard of Nuclear Facilities in Taiwan Using SSHAC Level 3 Methodology Project. Available at: <http://sshac.ncree.org.tw> (accessed 31 December 2019).
- Nguyen-Van, H., Phong, T.V., Trinh, P.T., Liem, N.V., Thanh, B.N., Pham, B.T., Bui, D.T., Bieu, N., Vinh, H.Q., Xuyen, N.Q., Tuc, N.D., Thom, B.V., Thuan, N.V., Thao, B.T., Phong, L.H., Vinh, V.D., Tan, M.T., Hai, V.Q., Lan, N.M., Cuong, T.Q., Hang, P.T.T., Ha, V.V., Hoang, C.M., Hao, D.V., Son, T.P.H., 2020. Recent tectonics, geodynamics and seismotectonics in the Ninh Thuan Nuclear Power plants and surrounding regions, South Vietnam. *J. Asian Earth Sci.* 187, 104080. <https://doi.org/10.1016/j.jseas.2019.104080>.
- Nguyen, H.P., Pham, T.T., Nguyen, T.N., 2019. Investigation of long-term and short-term seismicity in Vietnam. *J. Seismolog.* 23 (5), 951–966.
- Nguyen, L.M., Lin, T.-L., Wu, Y.-M., Huang, B.-S., Chang, C.-H., Huang, W.-G., Le, T.S., Nguyen, Q.C., Dinh, V.T., 2012. The first peak ground motion attenuation relationships for North of Vietnam. *J. Asian Earth Sci.* 43, 241–253.
- Nguyen, D.X., Le, T.S., 2005. Seismic hazard assessment for Vietnam Territory. In: *Proceeding of the 4th Conference of Vietnamese Association of Geophysics*. Publishing House of Science and Technology, Hanoi, Vietnam, pp. 281–304.
- Nguyen, V.-D., Huang, B.-S., Lai, Y.-C., Nguyen, L.M., Le, T.-S., Dinh, V.-T., Wen, K.-L., Lai, H.-P., 2020. Deep crust analysis beneath northern Vietnam by using receiver functions: Implications for SE Asia continental extrusion. *Terrestrial, Atmospheric & Oceanic Sci.* 31 (4), 453–468.
- Nguyen, V.-D., Huang, B.-S., Le, T.-S., Dinh, V.-T., Zhu, L., Wen, K.-L., 2013. Constraints on the crustal structure of Northern Vietnam based on analysis of teleseismic converted waves. *Tectonophysics* 601, 87–97.
- Pailoplee, S., Choowong, M., 2014. Earthquake frequency-magnitude distribution and fractal dimension in mainland Southeast Asia. *Earth Planets Space* 66 (1), 8. <https://doi.org/10.1186/1880-5981-66-8>.
- Truyen, P.T., Phuong, N.H., 2019. Probabilistic seismic hazard assessment for Hanoi city. *Vietnam J. Earth Sci.* 41 (4), 321–338.
- Phan, D.P., Tokarski, A.K., Świerczewska, A., Strzelecki, P.J., Waliczek, M., Krapiec, M., Cuong, N.Q., 2019. Neotectonic (Miocene to recent) vertical movements in the Lao Cai Basin (Red River Fault Zone, Vietnam): An approach to seismic hazard assessment. *J. Asian Earth Sci.* 181, 103885. <https://doi.org/10.1016/j.jseas.2019.103885>.
- Phung, V.-B., Loh, C.H., Chao, S.H., Chiou, B.S.J., Huang, B.-S., 2020. Ground motion prediction equation for crustal earthquakes in Taiwan. *Earthquake Spectra* 36 (4), 2129–2164.
- Phuong, Nguyen Hong, 1991. Probabilistic assessment of earthquake hazard in Vietnam based on seismotectonic regionalization. *Tectonophysics* 198 (1), 81–93.
- Replumaz, A., Lacassin, R., Tapponnier, P., Leloup, P.H., 2001. Large river offsets and Plio-Quaternary dextral slip rate on the Red River fault (Yunnan, China). *J. Geophys. Res. Solid Earth* 106 (B1), 819–836.
- Robinson, D.P., Das, S., Searle, M.P., 2010. Earthquake fault superhighways. *Tectonophysics* 493 (3–4), 236–243.
- Tapponnier, P., Peltzer, G., Le Dain, A.Y., Armijo, R., Cobbold, P., 1982. Propagating extrusion tectonics in Asia: New insights from simple experiments with plasticine. *Geology* 10 (12), 611. [https://doi.org/10.1130/0091-7613\(1982\)10<611:PETIAN>2.0.CO;2](https://doi.org/10.1130/0091-7613(1982)10<611:PETIAN>2.0.CO;2).
- Hung, T.V., Kiyomiya, O., 2012. Ground motion attenuation relationship for shallow strike-slip earthquakes in Northern Vietnam Based on Strong motion records from Japan, Vietnam and adjacent regions. *J. Japan Society Civil Engineers, Ser. A1 (Structural Engineering & Earthquake Eng. (SE/EE))* 68 (3), 509–525.
- Hung, T.V., Kiyomiya, O., 2013. Source Parameter Estimation and Stochastic Ground Motion Simulation Based on Recorded Accelerograms in Northwestern Vietnam. *J. Earthquake Eng.* 17 (3), 304–322.
- Trần, D.T., Nguyễn, T.Y., Dương, C.C., Vy, Q.H., Zuchiewicz, W., Nguyễn, Q.C., Nguyễn, V.N., 2013. Recent crustal movements of Northern Vietnam from GPS data. *J. Geodyn.* 69, 5–10.
- Trinh, P.T., Van Liem, N., Van Huong, N., Vinh, H.Q., Van Thom, B., Thao, B.T., Tan, M. T., Hoang, N., 2012. Late Quaternary tectonics and seismotectonics along the Red River fault zone, North Vietnam. *Earth Sci. Rev.* 114, 224–235.
- Tuyen, N.H., Lu, N.T., 2012. Recognition of earthquake-prone nodes, a case study for North Vietnam ( $M \geq 5.0$ ). *Geod. Geodyn.* 3 (2), 14–26.
- Vackár, J., Burjánek, J., Gallovič, F., Zahradník, J., Clinton, J., 2017. Bayesian ISOLA: new tool for automated centroid moment tensor inversion. *Geophys. J. Int.* 210 (2), 693–705.
- Vavryčuk, V., 2014. Iterative joint inversion for stress and fault orientations from focal mechanisms. *Geophys. J. Int.* 199 (1), 69–77.
- Wan, Y., Sheng, S., Huang, J., Li, X., Chen, X., 2016. The grid search algorithm of tectonic stress tensor based on focal mechanism data and its application in the boundary zone of China, Vietnam and Laos. *J. Earth Sci.* 27, 777–785.
- Wu, W.-J., Wen, S., Tang, C.-C., Yeh, Y.-L., Lai, H.P., Dinh, V.T., Chen, C.-H., 2018. Seismogenic Structures in the Ma River Fault Zone, Vietnam: Insights from Focal Mechanisms of Microearthquakes and Local Stress States. *Bull. Seismol. Soc. Am.* 108 (6), 3260–3269.
- Zhao, J.X., Irikura, K., Zhang, J., Fukushima, Y., Somerville, P.G., Asano, A., Ohno, Y., Oouchi, T., Takahashi, T., Ogawa, H., 2006. An empirical site-classification method for strong-motion stations in Japan using H/V response spectral ratio. *Bull. Seismol. Soc. Am.* 96, 914–925.
- Zuchiewicz, W., Cuong, N.Q., Bluszcz, A., Michalik, M., 2004. Quaternary sediments in the Dien Bien Phu fault zone, NW Vietnam: a record of young tectonic processes in the light of OSL-SAR dating results. *Geomorphology* 60 (3–4), 269–302.
- Zuchiewicz, W., Cu'ò'ng, N.Q., Zasadni, J., Yèm, N.T., 2013. Late Cenozoic tectonics of the Red River Fault Zone, Vietnam, in the light of geomorphic studies. *J. Geodyn.* 69, 11–30.